Journal of Applied Physics

RESEARCH ARTICLE | NOVEMBER 20 2024

Field emission from cylindrical graphene cathodes prepared by chemical vapor deposition and cold rolling

Nathaniel Hernandez ; Renato Piovesan Azambuja ; Marc Cahay ; Jonathan Ludwick ; Tyson Back ; Ayush Raut ; Maliha Marzana ; Vamsi Krishna Reddy Kondapalli ; Qichen Fang ; Vesselin Shanov

J. Appl. Phys. 136, 195107 (2024)
https://doi.org/10.1063/5.0232314

Journal of Applied Physics ARTICLE pubs.aip.org/aip/jap

Field emission from cylindrical graphene cathodes prepared by chemical vapor deposition and cold rolling

Cite as: J. Appl. Phys. **136**, 195107 (2024); doi: 10.1063/5.0232314
Submitted: 6 August 2024 · Accepted: 5 November 2024 ·
Published Online: 20 November 2024

Nathaniel Hernandez,[1,2] Renato Piovesan Azambuja,[1] Marc Cahay,[1,2,a)] Jonathan Ludwick,[3] Tyson Back,[3] Ayush Raut,[4] Maliha Marzana,[4] Vamsi Krishna Reddy Kondapalli,[4] Qichen Fang,[5] and Vesselin Shanov[4,5]

AFFILIATIONS

[1]Electrical and Computer Engineering, Vacuum Nanoelectronics Laboratory, University of Cincinnati, Cincinnati, Ohio 45221, USA
[2]UES, A BlueHalo Company—4401 Dayton-Xenia Rd, Dayton, Ohio 45432, USA
[3]Air Force Research Laboratory, Materials and Manufacturing Directorate, Wright-Patterson Air Force Base, Ohio 45433, USA
[4]Mechanical and Materials Engineering, Nanoworld Laboratory, University of Cincinnati, Cincinnati, Ohio 45221, USA
[5]Chemical and Environmental Engineering, Nanoworld Laboratory, University of Cincinnati, Cincinnati, Ohio 45221, USA

[a)]**Author to whom correspondence should be addressed:** cahaymm@ucmail.uc.edu

ABSTRACT

We report field emission (FE) properties of cold cathodes made by a scalable chemical vapor deposition synthesis of three-dimensional graphene (3DG) from a cast catalyst followed by cold rolling. This process leads to an increase in mechanical strength and electrical conductivity of the tested material. For a given distance between the tip of the cathode and the anode, it is found that the FE current from the edge of a single sheet of cold-rolled 3DG-based cathode can be increased by over one order of magnitude when rolling the 3DG sheet in the shape of a cylinder with several turns. A FE current in the order of 4.5 mA was measured from a 3 mm diameter cold-rolled 3DG cylinder with six turns at a bias of 2400 V for a separation of 0.5 mm between the tip of the cylindrical cathode and the anode. The FE data of all cold-rolled 3DG-based cathodes are well fitted by the expression proposed by Abbot, Henderson, Forbes, and Popov [Filippov *et al.*, R. Soc. Open Sci. **9**, 220748 (2022)], $I_m = CV_m^{\kappa}\exp(-B/V_m)$, where I_m is the FE current, V_m is the bias applied between the cathode and anode, and B and C are fitting parameters. It is found that $\kappa = 1$ and $3/2$ for FE from the surface and edge of the cold-rolled based cathodes, respectively.

I. INTRODUCTION

Field emission (FE) cold cathodes have received widespread attention for applications in electron microscopy, electron beam lithography, novel x-ray sources, vacuum electronic devices, terahertz sources, and high-power microwave tubes. For these applications, cathodes need to generate electron beams exhibiting long lifetime when subjected to damaging conditions such as ion back-bombardment and intense heating.

The most widely used cold cathode material for high power microwave (HPM) devices is carbon fiber velvet.[1–6] In the past, carbon nanotube fibers have demonstrated improved performance over carbon fibers during direct current (DC) FE mode of operation.[7–12] More recently, graphene-based materials have also been investigated for use as FE cathodes in HPM devices, particularly for those requiring a large area or conformable cathode surface.[13–35] A variety of graphene-based materials has been reported in recent years; however, combining their excellent mechanical and electrical properties in a bulk form has not been entirely achieved. Over the last 15 years, there have been several reports on the FE properties of single- and few-layer graphene sheets and graphene sheet arrays in direction perpendicular or in the plane of the sheets. Chen *et al.*[25] published a review article

describing many attempts to fabricate graphene or reduced graphene oxide field emitters using various methods such as chemical vapor deposition, chemical exfoliation, electrophoretic deposition, screen-printing, and chemical synthesis methods. These studies have shown that the vertical alignment of graphene sheets or edge arrays can facilitate efficient electron emission from the atomically thick sheets. These arrays have been shown to possess a low turn-on voltage, high field enhancement factor, current stability, and luminance.

The pristine and cold-rolled graphene samples are composed of multilayered graphene flakes which are randomly oriented. The flakes close to the emitting edge of the graphene sheets are those which participate in FE. The large field enhancement factor of these flakes is what causes FE from their edges. For the cold-rolled samples, there may be some electrostatic screening of the field enhancement factor by the flakes which are in close proximity. The great number of flakes near the edge is what eventually leads to a large FE current from the cold-rolled samples. For instance, Gao and Okada[36] recently wrote a review of FE from graphene nanostructures pointing out that emission occurs mainly at the edge of the graphene flakes where electric field lines are highly concentrated making emission current very sensitive to the flake edge's geometry and their functionalization.[22] Zhang *et al.*[37] showed that graphene emitters may feature sharp protruded tips, increasing the field enhancement factor by upwards of a factor of 6. Zhang *et al.*[38] examined vertical few-layer graphene and demonstrated how the geometry of the emitter (height and tip shape) greatly affect the field emission performance. Hu *et al.*[39] investigated the field screening effect on graphene nanoribbons, showing how the enhancement factor depends on both the ribbon width and distance between ribbons.

FE from graphene is still a challenge because the fabrication methods such as micro-mechanical exfoliation, screen-printing, and electro-chemical deposition, can result in sheets lying flat on the substrate which is disadvantageous for electron tunneling from the surface barrier.[40] Liquid-phase exfoliation can be utilized to achieve bulk graphene sheet field emitters; however, the shapes are not uniform with a random distribution and require transfer techniques, which limits any practical FE properties. For instance, the screen-printing method is a simple technology for the preparation of large-scale graphene FE cathodes, but organic binders mixed with graphene during the fabrication process can result in high emitter and contact resistance. To date, several other methods have been developed to design and fabricate graphene for potential applications as a field emitter. However, the low-cost, large-area, high quality, and yield of the products are still far away from the practical FE applications.[36] The fabrication of graphene with optimized sizes, controllable shapes, high electrical conductivity, and stability remains a challenge in expanding its fundamental properties and potential applications. From a technological point of view, both an ultra-high and stable emission current density along with reproducible performance are necessary to satisfy commercial applications. To meet these demands, alignment uniformity, tailoring the density and shape of the emitters, along with optimizing the intrinsic properties such as work function and conductivity are needed to improve the FE performance.

In this work, we investigate how our recent advances in producing and characterizing three-dimensional graphene (3DG) can help address these challenges; 3DG has become an area of great interest due to its unique properties, different synthesis routes, and structures, as described in the literature. The challenges of retaining high quality, scaling up fabrication, and proven feasibility are apparent. In the past, we have investigated the synthesis, processing, and applications of 3DG, and revealed a new architecture of this material obtained after cold rolling.[41–43] We also demonstrated how this novel form of cold-rolled 3DG structures offers an alternative to knitted carbon nanotube fabric cathodes,[12] which would need less tedious steps for fabrication and implementation in HPM devices, particularly for those requiring confined conformable cathode surfaces.

For a given distance between the tip of the cathode and the anode and a given applied bias, it is found that the FE current from the edge of a single sheet of cold-rolled 3DG cathode can be increased by one order of magnitude when rolling the 3DG sheet in the shape of a cylinder with several turns. A FE current of the order of 4.5 mA was measured from a 3 mm diameter cold-rolled 3DG cylinder with six turns at a bias of 2400 V and a separation of 0.5 mm between the tip of the cylindrical cold-rolled 3DG cathode and the anode.

Section II presents details of the preparation of cylindrical cathodes made of cold-rolled 3DG sheets. Section III describes the FE system used to record the FE data of the fabricated cold-rolled 3DG cathodes. Section IV reports the FE data from these cathodes and an analysis of their FE characteristics. Section V contains a discussion of the FE results, including a study of the stability of the FE current over a period of several hours. Finally, Section VI contains the conclusions of this work.

II. CATHODE DESIGN AND FABRICATION

Previously, we reported a new architecture of 3DG which has been achieved by cold rolling that yielded increase in its strength and electrical conductivity.[41–43] The fabrication process of the pristine 3DG sheet and the following cold rolling is illustrated in Fig. 1. It consists of the following steps:

Catalyst preparation. A catalyst slurry has been formed by dissolving polystyrene in toluene. The mixture was heated to 70°C and stirred until the polymer was completely dissolved. Then nickel powder as well as di-(ethylene glycol) dibenzoate serving as a plasticizer, were added and mechanically agitated until the nickel powder was well dispersed in the solution.

Knife casting An adjustable 150 mm wide casting knife applicator for film formation was employed. The prepared mixture was poured behind the knife on a flat, smooth, and leveled Teflon sheet. The blade was then carefully guided over the thicker slurry, producing a film with customizable thickness, depending on the height of the knife. The cast slurry was left in a ventilated area until the toluene evaporated, leaving a flexible film of nickel–polymer composite held together by the polystyrene binder. The graphene sheets prepared this way can be tailored in any design dimensions and cut by a roll blade, scissors, or laser, then placed in a CVD reactor for the synthesis of pristine 3D graphene. Synthesis and post-processing The

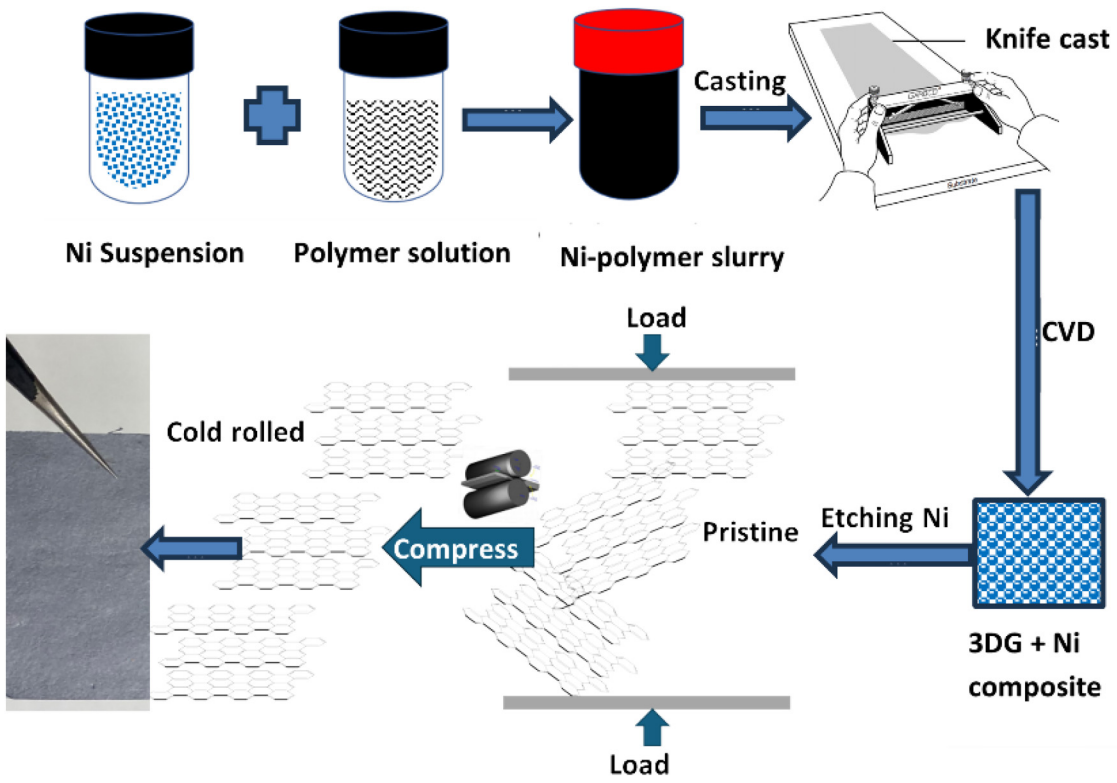

FIG. 1. Schematic illustrating the fabrication of pristine 3DG by CVD followed by cold rolling.[42,44]

chemical vapor deposition (CVD) synthesis was carried out in a ET-1000 First Nano reactor containing a quartz tube ($1000 \times 50\,mm^2$), and a flat quartz platform ($200 \times 20\,mm^2$) suspended in the tube by a loading arm. The CVD process was carried out at 1000°C in the presence of an argon, hydrogen, and methane gas mixture at volumetric flow rates of 1000, 325, and 25 SCCM, respectively. After three minutes of such processing, the reactor was cooled rapidly in the presence only of argon and hydrogen. Once the sample has reached room temperature following the forced cooling, the formed porous Ni-graphene substance was removed from the reactor and then submerged in a heated hydrochloric acid bath, 50% by volume, at 80°C for 4 h to extract the remaining Ni. The sample was then rinsed several times with DI water until reaching a pH of 7 and transferred into a container where a final wash with ethanol has been conducted followed by drying in air. Details related to the processing steps can be found elsewhere.[41]

Images of the surface and cross-sectional morphology of pristine and cold-rolled 3DG obtained by SEM are displayed in Fig. 2. The compression of pristine 3DG caused its thickness reduction along with folding, stacking, and alignment of the graphene flakes parallel to the surface. This can increase the mean free path of the electrons thus raising the electrical conductivity of compressed samples which can reach values in excess of 1000 °S/cm.[42,44]

III. DC FE TESTING

DC FE measurements were performed in a custom made UHV chamber built by McAllister Technical Services. This system was used in the past to study the FE characteristics of CNT based straight and looped fibers and CNT films.[12,45–48] Measurements were made at a background pressure of 10^{-8} Torr in a diode configuration. All samples were let to degas in the vacuum chamber for a period of two days prior to making FE measurements. In our setup, a 5 mm diameter stainless steel anode probe tip is driven by a stepper motor with a 2.5 μm step size for controlling the anode–cathode gap distance. The pristine or cold-rolled 3DG sheets are mounted to a stainless-steel rail on an XY axis linear translation stage. Centering the anode tip over the individual vertically oriented graphene samples is accomplished by an XY axis linear translation stage with the use of two optical cameras looking through viewports positioned at 90° from each other in the same plane.

The FE properties of cold-rolled 3DG sheets placed either in the plane of the cathode or aligned in a direction perpendicular to it have been investigated. An Infinity SK Long Distance Microscope with a C4 objective is used for imaging the cold-rolled 3DG cathode and the anode-cathode gap distance. Once the gap distance

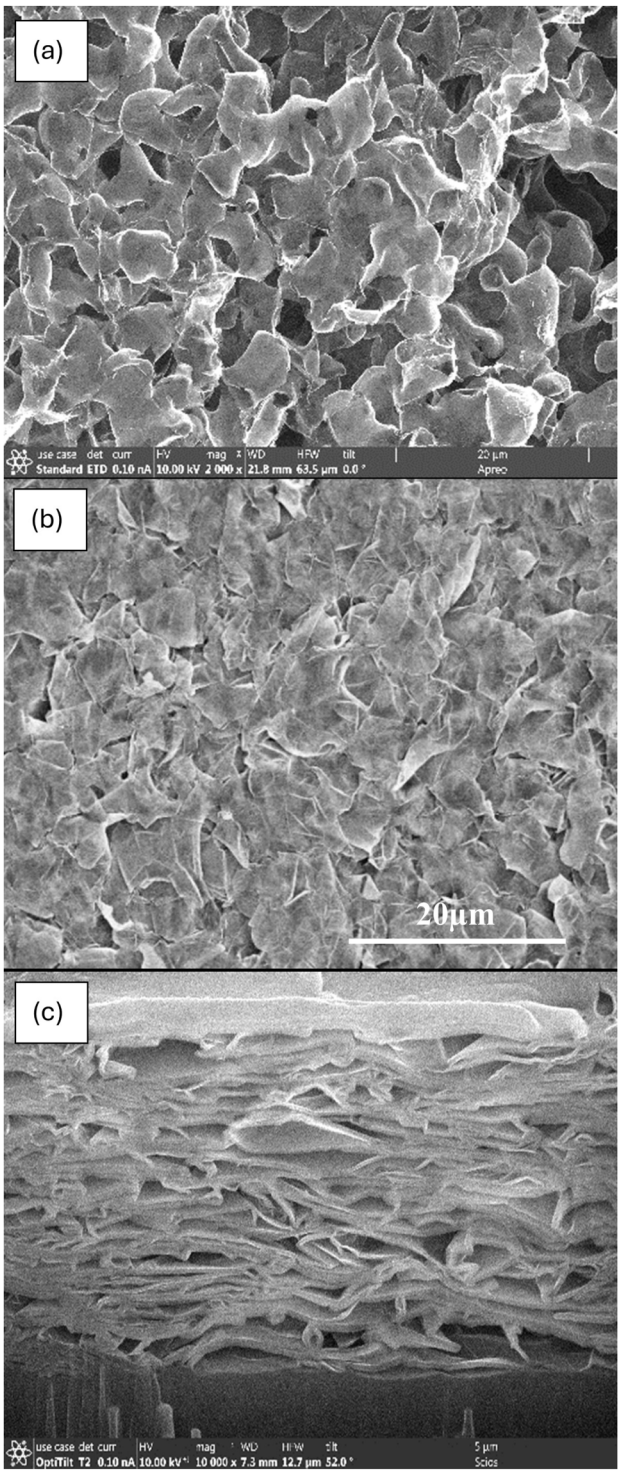

FIG. 2. SEM images of: (a) pristine 3DG surface, (b) cold-rolled 3DG surface, (c) cross section of cold-rolled 3DG with a thickness of 15.2 μm cut by FIB perpendicular to the rolling direction.[42,44]

is set, the voltage on the anode is increased in steps ranging from 1 to 10 V every second up to 3000 V with a Keithley 6517A source meter. Increasing the voltage in this manner allows the sample to outgas properly. FE data are recorded at each voltage by a computer running LabVIEW. Bonding of the cold rolled 3DG sheets to the substrate was achieved with a conductive silver paint.

The conditioning of each cathode consists of ramping the applied voltage up to a certain voltage $V_{\max}$ and back down, gradually increasing $V_{\max}$ with each sweep until reaching the desired maximum voltage. During this process, the cathode may exhibit sporadic FE characteristics, with periods of low and high current and abrupt transitions between them. Additionally, the cathode may display loop-type characteristics resembling hysteresis between the upward and downward sweeps. Once the conditioning reaches the desired voltage, the voltage is swept repeatedly until the cathode exhibits consistent FE behavior, usually requiring only two or three sweeps. The FE data reported hereafter are those observed during the final third of the up and down sweeps.

In Sec. IV, it is shown that for sufficient large values of the applied bias, the FE characteristics of the various cold-rolled 3DG cathodes are well fitted by a mathematical expression recently proposed by Abbot–Henderson–Forbes–Popov (referred hereafter as the AHFP equation),[49]

$$I_m = CV_m^{\kappa}\exp(-B/V_m), \tag{1}$$

where I_m is the FE current, V_m is the bias applied between the cathode and anode, and B and C are fitting parameters. The fitting of the forward bias current data was done using a MATLAB subroutine to perform a combination of global searching and least squares fitting of the log of the emission current vs applied bias.[50]

A recent analytical model of electrostatic FE tunneling from the edge and surface of two-dimensional materials leads to a universal scaling between the tunneling current density and electric field near the barrier characterized by a line with a negative slope in the generalized MG plot of $\ln(J/V^{\kappa}) \sim 1/V$. Ang *et al.*,[51] showed that $\kappa = 3/2$ and $\kappa = 1$ for FE from the edge and surface of 2D materials, respectively. These theoretical results are used hereafter to analyze the FE data for several cold-rolled 3DG cathodes.

IV. RESULTS

The FE characteristics of the various cold-rolled 3DG cold cathodes were recorded by sweeping the anode voltage from 0 V to a maximum voltage $V_{\max}$ on the anode followed by a reverse sweep from V_{max} down to 0 V. Unless otherwise stated, there was no dwell time period at which the maximum voltage was held constant between the forward and reverse sweeps. The up and down sweeps were recorded by a change in the voltage in steps of 10 V every second. To condition the cathode, the maximum voltage on the anode was gradually increased and, for a given maximum voltage, several up- and down-sweeps were recorded. The FE data shown hereafter are the data obtained after no substantial change was seen between the successive up- and down-sweeps.

Figure 4 shows the FE characteristics of a cold-rolled 3DG sheet placed horizontally on top of a copper plate attached to the

cathode chuck, as shown in Fig. 3(a). The cold-rolled 3DG cathode was held in place using a plastic holder with four screws to ensure firm contact of the graphene sheet to the bottom copper plate to which it is glued using a silver conductive paint. The opening in the plastic holder is about 1 cm^2 which is large enough to control the placement of the 5 mm diameter anode on top of the cathode. The top and bottom frames in Fig. 4 shown a linear and MG plots of the FE data, respectively. In the MG plot, since the FE current is in a direction perpendicular to the plane of the graphene sheet, a value of $\kappa = 1$ was used in Eq. (1) to fit the FE data.[51] The straight line in the MG plot shows the fit to the FE data for large values of the applied bias. A maximum FE current of 70μA at 2800 V was observed for a distance of 0.5 mm between the plane of the cathode and the anode. Since the anode has a 5 mm diameter, this corresponds to a maximum macroscopic emission current density of 0.4 mA/cm^2, which is of the same order of magnitude as the maximum current density in the direction perpendicular to other graphene sheet emitters.[25] The near linear behavior of the FE data at high applied voltage in the MG plot is evidence of the successful demonstration of FE mode of operation of this cold-rolled 3DG horizontal cathode.

As seen in Fig. 4, there is a small loop-type behavior in the FE data with the FE current being slightly larger in the up-sweep than in the down-sweep. When operating the cathode at large applied bias, some sparks were observed near the surface of the cathode which could be attributed to partial destruction of some of the graphene flakes at the top of the horizontal emitter, and may be due to increased self-heating effects in some of the flakes. This would indeed to a lesser number of flakes contributing to the FE current on the down-sweep and the observed loop-type behavior in the FE characteristics. Alternatively, it has been shown that some graphene and other carbon cathodes have demonstrated self-assembly during operation which rebuilds the cathode continuously. The loop-behavior in the FE data could also be due to localized exfoliation of carbon and contaminants during FE. This may cause ionization and subsequently bombardment on the emission edge, restructuring the surface with numerous graphene flakes, as was observed for other types of cathodes.[52–58] The investigation of the origin of the loop-behavior in the FE data will require a more thorough investigation.

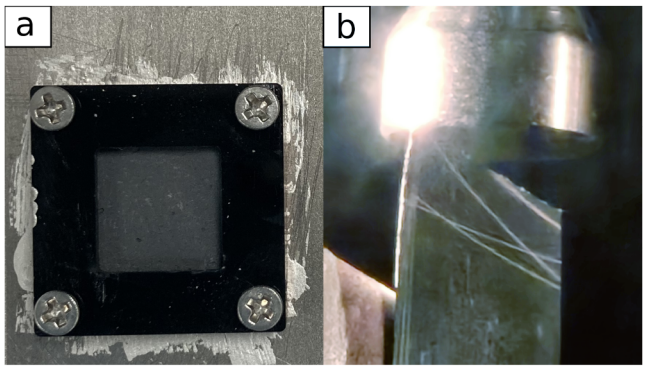

FIG. 3. Optical images of cold-rolled 3D graphene sheets mounted (a) horizontally on top of a copper cathode and (b) vertically on the side of a copper block.

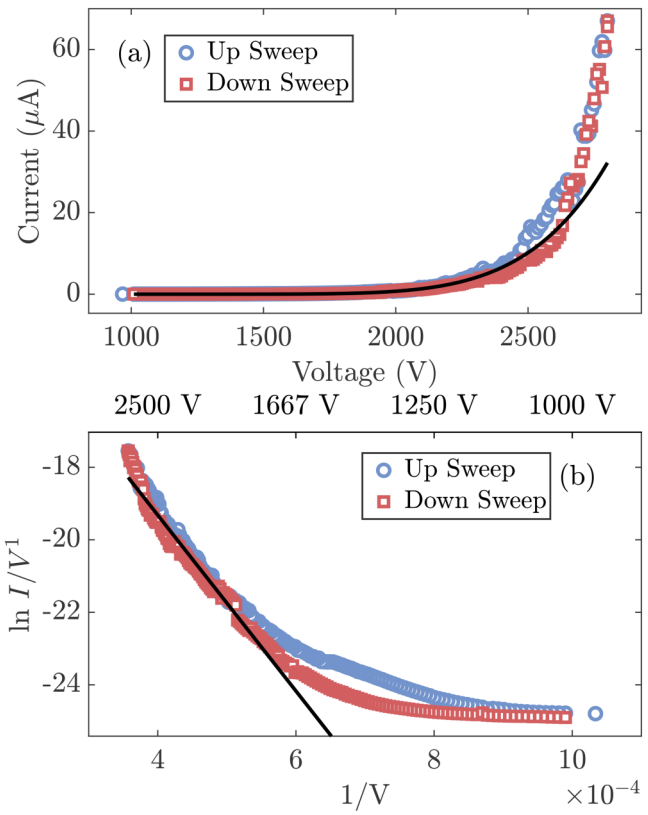

FIG. 4. (a) FE characteristics from a cold-rolled 3DG graphene sheet mounted horizontally on a copper cathode. The inset shows the cold-rolled 3DG graphene sheet with an area of 1 cm^2. The separation between the top of the cold-rolled 3DG sheet and the anode was set to 500 μm; (b) MG plot of the FE data. The straight line is a fit to the up-sweep FE data for large values of the applied bias.

Figure 5 shows the FE data (both linear and MG plots) of a square cold-rolled 3DG graphene sheet about 2 cm on a side mounted vertically on the edge of a copper block attached to the cathode. Figure 3(b) shows the anode about 0.5 mm above the top of the edge of the 3DG sheet. In this case, a maximum of 0.14 mA was recorded at a maximum voltage on the anode of 2500 V. The MG plot is linear for large values of the applied bias which is evidence of successful FE from the edge of the 3DG graphene sheet. Since the FE is measured from the edge of the graphene sheet, a value of $\kappa = 3/2$ was used on the MG plot of the FE data. In Fig. 5(b), the straight line is a fit to the FE data for large values of the applied bias using Eq. (1). As in the case of the horizontal 3DG cathode, the FE data in the forward sweep are larger than for the reverse sweep, which may be attributed to the partial destruction of graphene flakes due to self-heating effects or restructuring of some of the graphene flakes near the tip of the cathode. A more thorough analysis would require taking SEM pictures of the tip of the cathode before and after collecting the FE data.

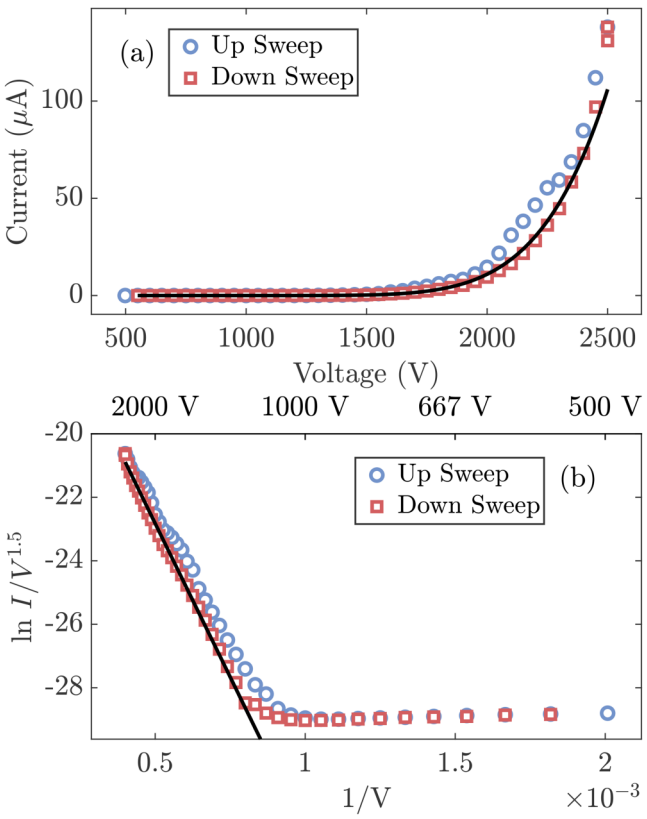

FIG. 5. (a) FE data from the edge of a cold-rolled 3D graphene sheet mounted vertically on the side of a copper block with a 500 μm gap between top of the graphene sheet and the anode; (b) MG plot of the FE data. The straight line is a fit to the up-sweep FE data for large values of the applied bias using Eq. (1).

In order to increase the overall current, one could use an array of vertical cold-rolled 3DG sheets. Since the anode is only 5 mm in diameter, a new vertical cathode was formed by rolling a cold-rolled 3DG sheet into a spiral using the following procedure.

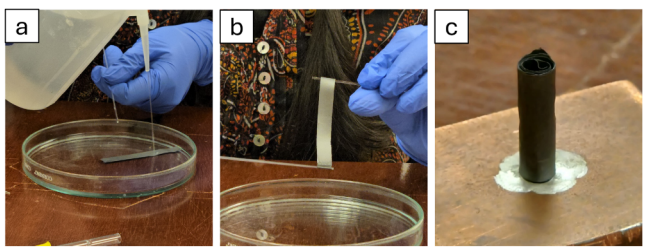

FIG. 6. (a) Preparation of cylindrical graphene emitter: soaking the 3DG sheet into ethanol; (b) picking one edge of the graphene sheet and rolling it around with tweezers; (c) picture of the cylindrical graphene emitter formed with six turns of the 3DG sheet and mounted on a copper block with a silver conductive paint.

A 1 cm wide and 15 cm long 3DG sheet was first soaked into ethanol, as shown in the left frame of Fig. 6(a). After picking up one edge of the graphene sheet with tweezers, it was rolled around a glass pipet about 1 mm in diameter acting as a support to form the graphene cylinder [Fig. 6(b)]. After rotating the graphene sheet six times around the glass pipet, the latter was extracted from the center of the 3DG graphene cylinder which was then mounted vertically on a copper block with a silver conductive paint and placed in the FE DC chamber for testing.

Figure 7 shows a comparison of the up-sweep FE data (both linear and MG plots) for the cold-rolled 3DG vertical emitter and the cylindrical cathode shown in Fig. 6(c) which contains six turns of the 3DG cold-rolled sheet. For both cathodes, the FE data were recorded with a distance between the top of the cathode and the anode set to 0.5 mm. In Fig. 7(b), the straight line is a fit to the FE data of the spiral emitter using Eq. (1). As in the case of the single sheet vertical emitter, a value of $\kappa = 3/2$ was used in the MG plot of the FE data for large values of the applied bias.

Over the anode bias range from 1000 to 2500 V, the FE current of the cylindrical shape cathode shown in Fig. 7 is about a

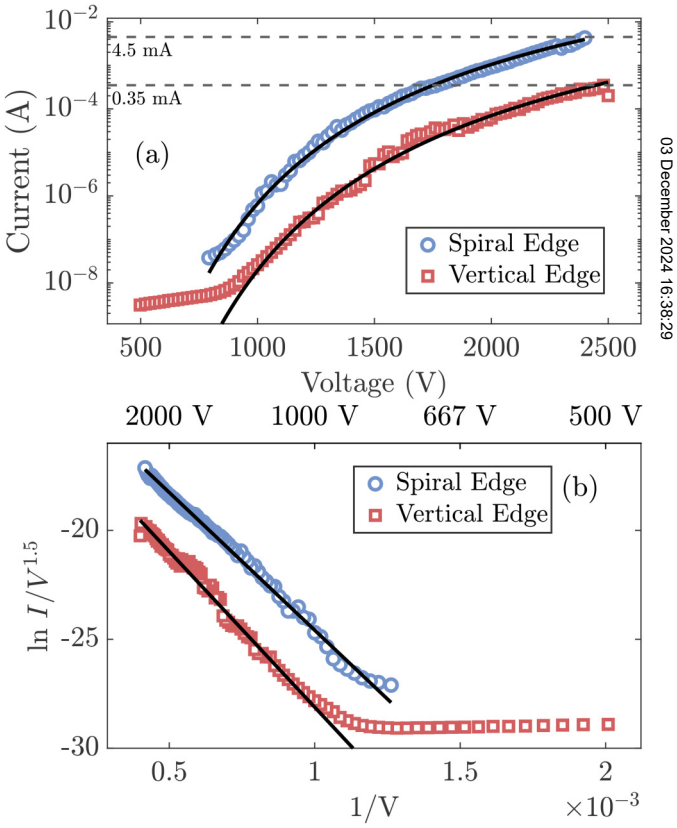

FIG. 7. Comparison of the FE data from the cold-rolled 3DG vertical emitters shown in Figs. 5 and 6 for a distance between the top of both cathodes and the anode set to 500 μm. The (a) top and (b) bottom frames are a linear and MG plot of the up-sweep FE data, respectively.

TABLE I. Extracted FE fitting parameters in Eq. (1) for the various orientations of the cold-rolled 3DG. The value of κ is set to be constant. The miminum distance between the cathode and anode gap was set to be 500 μm.

Orientation	ln(C)	B	κ	Max Current
Horizontal	−6.34	−32 460	1	0.07 mA @ 2800 V
Vertical	−13.15	−19 350	1.5	0.35 mA @ 2500 V
Spiral	−11.94	−12 640	1.5	4.5 mA @ 2400 V

factor 13 larger than for the edge emitter shown in Fig. 5. It is because different turns in the cylindrical cathode contribute to FE.

Table I lists the values of the fitting parameters in Eq. (1) for the various cold-rolled 3DG emitters described in this section. In all cases, the values of the parameter κ were held constant and the minimum distance between the cathode and the anode was set to 500 μm. Table I also lists the maximum current observed for each of the cold-rolled 3DG emitters.

V. DISCUSSION

A maximum current of the order of 4.5 mA was measured for the cylindrical emitter when there was no dwell time after the applied bias reached a maximum of 2400 V for a separation of 0.5 mm between the tip of the cylinder and the anode. Since the spiral emitter has 6 turns and a radius of 1.5 mm, the effective length of the spiral is about $6\pi r = 2.83$ cm. This corresponds to a maximum macroscopic linear FE current density of 1.6 mA/cm which is similar to the values reported for other graphene field edge emitters.[22] It is important to note that the FE from our cold-rolled 3D graphene samples is likely not uniform across the entire surface. The measurements presented here represent the macroscopic current density, which averages the emission current over the sample area. To study the non-uniformity of FE in future graphene samples, a phosphorescent screen could be employed. This technique would allow for direct visualization of emission hot spots and provide valuable insights into the spatial distribution of electron emission across the sample surface.

During the FE measurements on the cylindrical graphene cathode, some flashes were also observed from the top of the sheet forming the cathode for values of the applied bias above 2000 V. This led to morphological changes at the edges of the graphene sheet facing the anode. An optical micrograph from the top of the cylindrical graphene cathode obtained after FE is shown in Fig. 9(b). When testing the cylindrical graphene cold cathode, it was observed that it could emit a current of 5 mA which was the preset value of the compliance current in the experiments. It is therefore anticipated that cylindrical cathodes with more turns and designed with geometrical optimizations (e.g., 3DG spikes) could emit current of several tens of mA in the DC mode of operation.

To illustrate the onset of self-heating in the cylindrical cathode, Fig. 8 shows the time evolution of the FE current when raising the voltage on the anode to a maximum value over a period of 100 s, then holding the maximum voltage for a dwell time of 600 s, before lowering back to voltage on the anode down to zero over a period of 100 s. From bottom to top, The three curves in

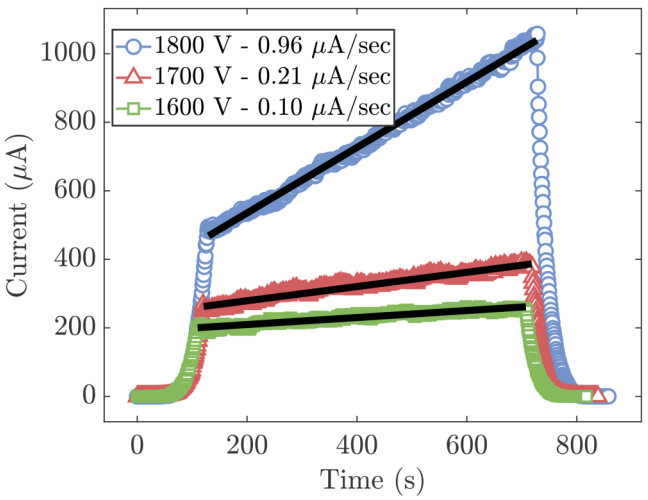

FIG. 8. Time dependence of the FE current for the cylindrical cathode for distance between tip of the cathode and anode of 500 μm. From bottom to top, the maximum anode voltage was held at 1600, 1700, and 1800 V for a period of 600,s.

Fig. 8 correspond to the cases where the maximum voltage on the anode is equal to 1600, 1700, and 1800 V. Figure 8 indicates that there is a monotonic increase of the FE current during the dwell time. The FE current increases by 0.06, 0.13, and 0.56 mA during the dwell time when the maximum voltage on the anode is set to 1600, 1700, and 1800 V, respectively. We attribute this increase to self-heating effects in the cathode which become more important as the maximum voltage on the anode increases. An alternative explanation for this behavior could be the adsorption of water or other species present in the vacuum chamber onto the surface of the 3DG emitter. This process could lower the work function, resulting in a gradual increase in current over time. To determine the exact cause of this phenomenon, further investigation is needed. Employing an infrared camera or thermocouple could help detect any self-heating effects, while a residual gas analyzer could identify the presence and nature of any adsorbed species. These tools would allow for a more comprehensive understanding of the underlying mechanisms driving the observed current increase.

Figure 9 shows optical images of the tip of the cylindrical cathode before and after FE measurements, clearly showing some damage near the top edge of the cathode. As mentioned above, this may be caused by self-assembly linked to localized exfoliation of carbon and contaminants during FE. This leads to ionization and subsequently bombardment of the emission edge, restructuring the surface with numerous flakes, as was observed by others groups for different types of graphene and carbon cathodes. SEM scans before and after would be giving more info about the destruction/restructuring of the graphene flakes near the tip of the cathode. This will be done in a later study.

Figure 10 shows the time evolution of the FE current of the spiral emitter for a separation of 0.5 mm between the tip of the emitter and the anode as the voltage on the anode was raised from

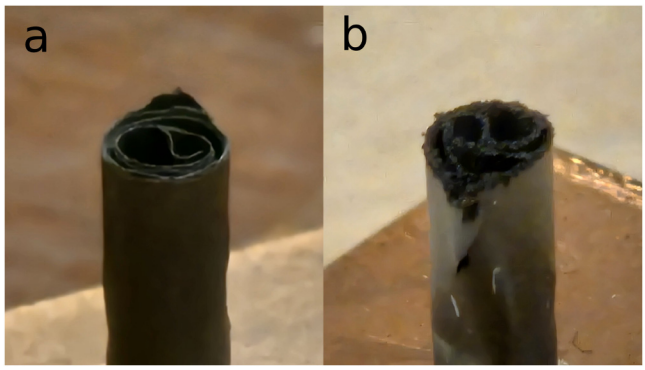

FIG. 9. Optical images of the tip of the cylindrical cathode (a) before and (b) after FE measurements.

0 V to a maximum of 1600 V in 120 s, then kept constant at 1600 V for 3 h, before being lowered from 1600 V down to 0 V in 120 s. Figure 10 shows the importance of self-heating effects in the spiral emitter as the FE current rises from 80 μA once the maximum anode voltage is reached to the fairly constant value of 400 μA during the 3 hour period when the voltage on the anode is held constant.

As shown in Fig. 10, when the applied bias of the anode is held at 1600 V, the time evolution of the FE current of the spiral emitter is well fitted by the following equation:

$$I(t) = I_0 + \Delta I\left(1 - \exp\left(\frac{-t}{\tau}\right)\right), \tag{2}$$

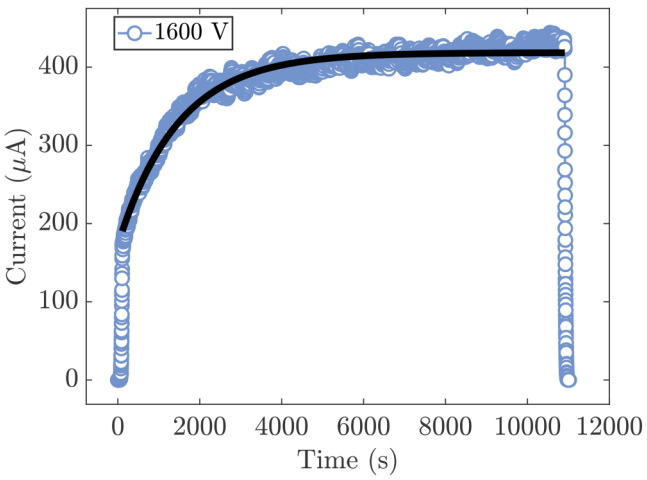

FIG. 10. Time evolution of the FE current of the cylindrical emitter for which the anode potential was held constant for 3 h after reaching a value of 1600 V. The distance between the anode and the tip of the cylindrical emitter was set to 0.5 mm. The full line shows the fit of the FE data using 2 over the 3 hour period during which the maximum potential on the anode was fixed.

for the following values of the fitting parameters: $I_0 = 172.4\,\mu$A, $\Delta I = 246.1\,\mu$A, and $\tau = 1464$ s. For this value of the anode bias, it takes about $5\tau = 7320$ s for the FE current to reach a steady state value.

VI. SUMMARY AND CONCLUSIONS

We have successfully fabricated new cold cathodes based on cold-rolled 3DG sheets which were obtained by a scalable CVD synthesis of three-dimensional graphene from a cast catalyst followed by cold rolling. The latter leads to an increase in the mechanical strength and electrical conductivity of the cold-rolled 3DG material. The FE data of all cold-rolled 3DG-based cathodes are well fitted by the expression proposed by Abbot, Henderson, Forbes, and Popov,[49] $I_m = CV_m^{\kappa}\exp(-B/V_m)$, where I_m is the FE current, V_m is the bias applied between the cathode and anode, and B and C are fitting parameters. It is found that $\kappa = 1$ and $3/2$ for FE from the surface and edge of the cold-rolled based cathodes, respectively.[51]

For a given distance between the tip of the cathode and the anode and a given applied bias, it is found that the FE current from the edge of a single sheet of cold-rolled 3DG cathodes can be increased by one order of magnitude when rolling the 3DG sheet in the shape of a cylinder with several turns. A FE current of 4.5 mA was measured from a 3 mm diameter and 1 cm tall 3DG cylinder with six turns at a bias of 2400 V and a separation of 0.5 mm between the tip of the cylindrical 3DG cathode and the anode.

The cylindrical cold-rolled 3DG cathode was built by rolling a long graphene sheet into a spiral with consecutive turns in close proximity. A recent numerical study of electrostatic shielding has been carried out by Yang *et al.*[24] which showed that a maximum emission efficient for an array of graphene sheets is achieved when the separation of the adjacent graphene sheets is four times the height of the individual sheets. Therefore, future studies of cold-rolled 3DG field emitters should include a flexible spacer between each turn of the spiral to minimize the effects of electrostatic shield between adjacent turns. This could be achieved by forming a spiral emitter starting with a bilayer of cold-rolled and thicker pristine graphene sheets. The cold-rolled sheet should be made higher than the pristine one so the field emission would mostly occur from the edge of the cold-rolled 3DG sheet.

Immediate applications of the proposed cold-rolled 3DG cathodes include FE sources in portable high-power microwave devices used in detection of chemical and biological agents in real-time, medical diagnostic imaging and long-distance communications for radar and electronic warfare for military and space operations. Other applications may include cathodes in flat-panel displays, electron-beam lithography, free-electron lasers, x-ray generation, electron microscopy, and ion-propulsion systems. Furthermore, 3DG sheet-based cold cathodes may replace the thermal electron emission cathodes used as electron sources for conduction-cooled superconducting accelerators.

ACKNOWLEDGMENTS

This work was supported by the Air Force Office of Scientific Research (Program Manager, Dr. Ken Goretta) under Award No.

FA9550-20RXCOR027 and by the UC Collaborative Research Advancement Grant No. 1018371. M.C. and N.H. acknowledge support of the Air Force Research Labs under Contract No. FA8650-22-F-5815. J.L. was supported by the Air Force Research Labs under Contract No. FA8650-22-F-5815. V.K.R.K. is thankful for the partial support by the National Institute for Occupational Safety and Health through Grant No.T42OH008432 from the Pilot Research Project Training Program of the University of Cincinnati (UC) Education and Research Center.

AUTHOR DECLARATIONS

Conflict of Interest

The authors have no conflicts to disclose.

Author Contributions

Nathaniel Hernandez: Conceptualization (equal); Data curation (equal); Formal analysis (equal); Investigation (equal); Methodology (equal); Resources (equal); Software (equal); Validation (equal); Visualization (equal); Writing – original draft (equal); Writing – review & editing (equal). **Renato Piovesan Azambuja:** Conceptualization (supporting); Data curation (supporting); Investigation (equal); Methodology (equal); Resources (equal); Validation (equal); Writing – review & editing (equal). **Marc Cahay:** Conceptualization (equal); Formal analysis (supporting); Funding acquisition (equal); Methodology (equal); Project administration (equal); Resources (equal); Software (supporting); Supervision (equal); Validation (equal); Visualization (equal); Writing – original draft (equal); Writing – review & editing (equal). **Jonathan Ludwick:** Conceptualization (supporting); Methodology (supporting); Resources (equal); Software (equal); Writing – review & editing (equal). **Tyson Back:** Conceptualization (supporting); Funding acquisition (equal); Methodology (supporting); Project administration (equal); Supervision (equal); Writing – review & editing (equal). **Ayush Raut:** Conceptualization (supporting); Methodology (supporting); Resources (equal); Writing – review & editing (equal). **Maliha Marzana:** Conceptualization (equal); Methodology (supporting); Resources (equal); Writing – review & editing (equal). **Vamsi Krishna Reddy Kondapalli:** Conceptualization (supporting); Methodology (supporting); Resources (supporting); Writing – review & editing (equal). **Qichen Fang:** Conceptualization (equal); Methodology (supporting); Resources (equal); Writing – review & editing (equal). **Vesselin Shanov:** Conceptualization (equal); Funding acquisition (equal); Methodology (equal); Project administration (equal); Resources (equal); Supervision (equal); Visualization (equal); Writing – original draft (equal); Writing – review & editing (equal).

DATA AVAILABILITY

The data that support the findings of this study are available from the corresponding author upon reasonable request.

REFERENCES

[1]T. Buntin, M. Abide, A. Neuber, J. Dickens, R. Joshi, and J. Mankowski, "Evaluation of explosive emission carbon fiber cathodes for high-power microwave devices," IEEE Trans. Plasma Sci. **50**, 3459–3467 (2022).
[2]D. Andreev, A. Kuskov, and E. Schamiloglu, "Review of the relativistic magnetron," Matter Radiat. Extrem. **4**, 067201 (2019).
[3]D. Shiffler, M. Ruebush, M. Haworth, R. Umstattd, M. LaCour, K. Golby, D. Zagar, and T. Knowles, "Carbon velvet field-emission cathode," Rev. Sci. Instrum. **73**, 4358–4362 (2002).
[4]D. Shiffler, M. Haworth, K. Cartwright, R. Umstattd, M. Ruebush, S. Heidger, M. LaCour, K. Golby, D. Sullivan, P. Duselis, and J. Luginsland, "Review of cold cathode research at the Air Force Research Laboratory," IEEE Trans. Plasma Sci. **36**, 718–728 (2008).
[5]B. W. Hoff, S. Beeson, D. Simon, W. Tang, R. Smith, S. C. Exelby, N. M. Jordan, A. Sayir, R. M. Gilgenbach, P. D. Lepell, and T. Montoya, "Brazed carbon fiber fabric field emission cathode," Rev. Sci. Instrum. **91**, 064702 (2020).
[6]Y. Sekii and T. Hayashi, "Measurements of reflectance and thermal emissivity of a black surface created by electrostatic flocking with carbon-fiber piles," IEEE Trans. Dielect. Electr. Insul. **16**, 649–654 (2009).
[7]N. Behabtu, C. C. Young, D. E. Tsentalovich, O. Kleinerman, X. Wang, A. W. K. Ma, E. A. Bengio, R. F. Ter Waarbeek, J. J. De Jong, R. E. Hoogerwerf, S. B. Fairchild, J. B. Ferguson, B. Maruyama, J. Kono, Y. Talmon, Y. Cohen, M. J. Otto, and M. Pasquali, "Strong, light, multifunctional fibers of carbon nanotubes with ultrahigh conductivity," Science **339**, 182–186 (2013).
[8]W. W. Tang, D. A. Shiffler, J. R. Harris, K. L. Jensen, K. Golby, M. LaCour, and T. Knowles, "Field emission characteristics of a small number of carbon fiber emitters," AIP Adv. **6**, 095007 (2016).
[9]J. Benford, J. A. Swegle, and E. Schamiloglu, "Introduction," in *High Power Microwaves*, 2nd ed. (CRC Press, 2007).
[10]D. Mihalcea, L. Faillace, J. Hartzell, H. Panuganti, S. Boucher, A. Murokh, P. Piot, and J. C. T. Thangaraj, "Measurement of Ampère-class pulsed electron beams via field emission from carbon-nanotube cathodes in a radiofrequency gun," Appl. Phys. Lett. **107**, 033502 (2015).
[11]D. Shiffler, O. Zhou, C. Bower, M. LaCour, and K. Golby, "A high-current, large-area, carbon nanotube cathode," IEEE Trans. Plasma Sci. **32**, 2152–2154 (2004).
[12]S. B. Fairchild, C. E. Amanatides, T. A. De Assis, P. T. Murray, D. Tsentalovich, J. L. Ellis, S. Portillo, S. R. Kanel, J. S. Bulmer, J. Park, G. Dion, and J. J. Boeckl, "Field emission cathodes made from knitted carbon nanotube fiber fabrics," J. Appl. Phys. **133**, 094302 (2023).
[13]J. Benford, J. A. Swegle, and E. Schamiloglu, "Vircators, Gyrotrons and Electron Cyclotron Masers, and Free-Electron Lasers," in *High Power Microwaves*, 2nd ed (CRC Press, 2007), Chap. 10.
[14]D. Price, D. Fittinghoff, J. Benford, H. Sze, and W. Woo, "Operational features and microwave characteristics of the Vircator II experiment," IEEE Trans. Plasma Sci. **16**, 177–184 (1988).
[15]H. A. Davis, R. R. Bartsch, L. E. Thode, E. G. Sherwood, and R. M. Stringfield, "High-power microwave generation from a virtual cathode device," Phys. Rev. Lett. **55**, 2293–2296 (1985).
[16]S. C. Exelby and C. J. Leach, "Advanced space charge limited field emission cathodes," Rev. Sci. Instrum. **94**, 104712 (2023).
[17]A.-K. Li, Y.-W. Fan, B.-L. Qian, Z.-C. Zhang, and T. Xun, "A low-outgassing-rate carbon fiber array cathode*," Chin. Phys. B **27**, 028401 (2018).
[18]Y. E. Krasik, J. G. Leopold, and U. Dai, "A relativistic magnetron operated with permanent magnets," IEEE Trans. Plasma Sci. **47**, 3997–4005 (2019).
[19]M. Haworth, K. Cartwright, J. Luginsland, D. Shiffler, and R. Umstattd, "Improved electrostatic design for milo cathodes," IEEE Trans. Plasma Sci. **30**, 992–997 (2002).
[20]D. Ye, S. Moussa, J. D. Ferguson, A. A. Baski, and M. S. El-Shall, "Highly efficient electron field emission from graphene oxide sheets supported by nickel nanotip arrays," Nano Lett. **12**, 1265–1268 (2012).

[21]S. W. Lee, S. S. Lee, and E.-H. Yang, "A study on field emission characteristics of planar graphene layers obtained from a highly oriented pyrolyzed graphite block," Nanoscale Res. Lett. **4**, 1218 (2009).
[22]V. I. Kleshch, D. A. Bandurin, A. S. Orekhov, S. T. Purcell, and A. N. Obraztsov, "Edge field emission of large-area single layer graphene," Appl. Surf. Sci. **357**, 1967–1974 (2015).
[23]S. Santandrea, F. Giubileo, V. Grossi, S. Santucci, M. Passacantando, T. Schroeder, G. Lupina, and A. Di Bartolomeo, "Field emission from single and few-layer graphene flakes," Appl. Phys. Lett. **98**, 163109 (2011).
[24]K. Yang, J. Liu, R. Jiang, Y. Gong, B. Zeng, J. Yang, F. Chi, and L. Liu, "Maximizing the field emission performance of graphene arrays," Nanomaterials **10**, 2003 (2020).
[25]L. Chen, H. Yu, J. Zhong, L. Song, J. Wu, and W. Su, "Graphene field emitters: A review of fabrication, characterization and properties," Mater. Sci. Eng. B **220**, 44–58 (2017).
[26]Y. Chen, J. Chen, and Z. Li, "Cold cathodes with two-dimensional van der Waals materials," Nanomaterials **13**, 2437 (2023).
[27]F. Giubileo, D. Capista, E. Faella, A. Pelella, W. Y. Kim, P. Benassi, M. Passacantando, and A. Di Bartolomeo, "Local characterization of field emission properties of graphene flowers," Adv. Electron. Mater. **9**, 2200690 (2023).
[28]N. Dwivedi, C. Dhand, J. D. Carey, E. C. Anderson, R. Kumar, A. K. Srivastava, H. K. Malik, M. S. M. Saifullah, S. Kumar, R. Lakshminarayanan, S. Ramakrishna, C. S. Bhatia, and A. Danner, "The rise of carbon materials for field emission," J. Mater. Chem. C **9**, 2620–2659 (2021).
[29]A. Patra, M. A. More, D. J. Late, and C. S. Rout, "Field emission applications of graphene-analogous two-dimensional materials: Recent developments and future perspectives," J. Mater. Chem. C **9**, 11059–11078 (2021).
[30]W. J. Chan, C. Chua, Y. S. Ang, and L. K. Ang, "Field emission in emerging two-dimensional and topological materials: A perspective," IEEE Trans. Plasma Sci. **51**, 1656–1670 (2023).
[31]C.-K. Huang, Y. Ou, Y. Bie, Q. Zhao, and D. Yu, "Well-aligned graphene arrays for field emission displays," Appl. Phys. Lett. **98**, 263104 (2011).
[32]S. Kumar, G. S. Duesberg, R. Pratap, and S. Raghavan, "Graphene field emission devices," Appl. Phys. Lett. **105**, 103107 (2014).
[33]Z. Yang, Q. Zhao, Y. Ou, W. Wang, H. Li, and D. Yu, "Enhanced field emission from large scale uniform monolayer graphene supported by well-aligned ZnO nanowire arrays," Appl. Phys. Lett. **101**, 173107 (2012).
[34]Z. Xiao, J. She, S. Deng, Z. Tang, Z. Li, J. Lu, and N. Xu, "Field electron emission characteristics and physical mechanism of individual single-layer graphene," ACS Nano **4**, 6332–6336 (2010).
[35]V. I. Kleshch, E. A. Vasilyeva, S. A. Lyashenko, I. V. Obronov, A. V. Tyurnina, and A. N. Obraztsov, "Surface structure and field emission properties of few-layer graphene flakes," Phys. Status Solidi (B) **248**, 2623–2626 (2011).
[36]Y. Gao and S. Okada, "Field induced electron emission from graphene nanostructures," Nano Ex. **3**, 034001 (2022).
[37]K. Zhang, S. Wu, X. Yang, B. Wang, W. Wu, J. Qian, W. Ou-Yang, R. Zhao, Y. Song, and Z. Sun, "Enhanced field emission properties of aligned sharp graphene emitter arrays prepared by freeze-drying and hydrothermal reduction," Mater. Res. Express **6**, 075608 (2019).
[38]Y. Zhang, J. Du, S. Tang, P. Liu, S. Deng, J. Chen, and N. Xu, "Optimize the field emission character of a vertical few-layer graphene sheet by manipulating the morphology," Nanotechnology **23**, 015202 (2011).
[39]H. Hu, T.-C. Lin, T.-C. Leung, and W.-S. Su, "Screening effects on the field enhancement factor of zigzag graphene nanoribbon arrays: A first-principles study," Phys. Chem. Chem. Phys. **20**, 14627–14634 (2018).
[40]W. Lv, L. Wang, Y. Lu, D. Wang, H. Wang, Y. Hao, Y. Zhang, Z. Sun, and Y. Tang, "A study on the field emission characteristics of high-quality wrinkled multilayer graphene cathodes," Nanomaterials **14**, 613 (2024).
[41]D. DeArmond, L. Zhang, R. Malik, K. Vamsi Krishna Reddy, N. T. Alvarez, M. R. Haase, Y.-Y. Hsieh, S. N. Kanakaraj, N. Oslin, J. Brunemann, J. Daum, and V. Shanov, "Scalable CVD synthesis of three-dimensional graphene from cast catalyst," Mater. Sci. Eng. B **254**, 114510 (2020).
[42]V. K. R. Kondapalli, G. Zhang, Y. Zhang, M. Khosravifar, K. Brittingham, N. Phan, S. Yarmolenko, J.-H. Bahk, and V. Shanov, "New architecture of 3D graphene with enhanced properties obtained by cold rolling," Carbon **207**, 116–128 (2023).
[43]V. K. R. Kondapalli, O. I. Akinboye, Y. Zhang, G. Donadey, J. Morrow, K. Brittingham, A. A. Raut, M. Khosravifar, B. Al-Riyami, J.-H. Bahk, and V. Shanov, "Three-dimensional graphene sheet-carbon veil thermoelectric composite with microinterfaces for energy applications," ACS Appl. Mater. Interfaces **16**, 13150–13160 (2024).
[44]V. K. R. Kondapalli, X. He, M. Khosravifar, S. Khodabakhsh, B. Collins, S. Yarmolenko, A. Paz y Puente, and V. Shanov, "CVD synthesis of 3D-shaped 3D graphene using a 3D-printed nickel–PLGA catalyst precursor," ACS Omega **6**, 29009–29021 (2021).
[45]S. B. Fairchild, J. S. Bulmer, M. Sparkes, J. Boeckl, M. Cahay, T. Back, P. T. Murray, G. Gruen, M. Lange, N. P. Lockwood, F. Orozco, W. O'Neill, C. Paukner, and K. K. K. Koziol, "Field emission from laser cut CNT fibers and films," J. Mater. Res. **29**, 392–402 (2014).
[46]M. Cahay, P. T. Murray, T. C. Back, S. Fairchild, J. Boeckl, J. Bulmer, K. K. K. Koziol, G. Gruen, M. Sparkes, F. Orozco, and W. O'Neill, "Hysteresis during field emission from chemical vapor deposition synthesized carbon nanotube fibers," Appl. Phys. Lett. **105**, 173107 (2014).
[47]S. B. Fairchild, J. Boeckl, T. C. Back, J. B. Ferguson, H. Koerner, P. T. Murray, B. Maruyama, M. A. Lange, M. M. Cahay, N. Behabtu, C. C. Young, M. Pasquali, N. P. Lockwood, K. L. Averett, G. Gruen, and D. E. Tsentalovich, "Morphology dependent field emission of acid-spun carbon nanotube fibers," Nanotechnology **26**, 105706 (2015).
[48]S. B. Fairchild, T. A. de Assis, J. H. Park, M. Cahay, J. Bulmer, D. E. Tsentalovich, Y. S. Ang, L. K. Ang, J. Ludwick, T. C. Back, and M. Pasquali, "Strongly anisotropic field emission from highly aligned carbon nanotube films," J. Appl. Phys. **129**, 125103 (2021).
[49]S. V. Filippov, A. G. Kolosko, E. O. Popov, and R. G. Forbes, "Field emission: Calculations supporting a new methodology of comparing theory with experiment," R. Soc. Open Sci. **9**, 220748 (2022).
[50]The MathWorks Inc., "Global Optimization Toolbox" (2023).
[51]L. K. Ang, Y. S. Ang, and C. H. Lee, "Universal model for electron thermal-field emission from two-dimensional semimetals," Phys. Plasmas **30**, 033103 (2023).
[52]S. Wu, Q. Wang, K. Guo, L. Liu, J. Bai, Z. Yang, X. Li, and H. Liu, "Synthesis and mechanism study of carbon nanowires, carbon nanotubes, and carbon pompons on single-crystal diamonds," Crystals **14**, 481 (2024).
[53]V. I. Kleshch, A. S. Orekhov, A. E. Pishchulina, I. V. Sapkov, D. N. Khmelenin, A. B. Loginov, R. R. Ismagilov, and A. N. Obraztsov, "All-carbon heterostructures self-assembly during field electron emission from diamond nanotip," Carbon **221**, 118936 (2024).
[54]A. Kyritsakis, E. Baibuz, V. Jansson, and F. Djurabekova, "Atomistic behavior of metal surfaces under high electric fields," Phys. Rev. B **99**, 205418 (2019).
[55]V. Jansson, E. Baibuz, A. Kyritsakis, S. Vigonski, V. Zadin, S. Parviainen, A. Aabloo, and F. Djurabekova, "Growth mechanism for nanotips in high electric fields," Nanotechnology **31**, 355301 (2020).
[56]X. Gao, A. Kyritsakis, M. Veske, W. Sun, B. Xiao, G. Meng, Y. Cheng, and F. Djurabekova, "Molecular dynamics simulations of thermal evaporation and critical electric field of copper nanotips," J. Phys. D: Appl. Phys. **53**, 365202 (2020).
[57]K. Kuppart, S. Vigonski, A. Aabloo, Y. Wang, F. Djurabekova, A. Kyritsakis, and V. Zadin, "Mechanism of spontaneous surface modifications on polycrystalline Cu due to electric fields," Micromachines **12**, 1178 (2021).
[58]G. Meng, Y. Li, R. A. Koitermaa, V. Zadin, Y. Cheng, and A. Kyritsakis, "*In situ* observation of field-induced nanoprotrusion growth on a carbon-coated tungsten nanotip," Phys. Rev. Lett. **132**, 176201 (2024).